Enzyme-degradable hybrid polymer/silica microbubbles as ultrasound contrast agents

Nadia H. Tsao, Elizabeth A. H. Hall*

Institute of Biotechnology, University of Cambridge

Tennis Court Road

Cambridge, CB2 1QT

Silica; PCL; Microbubbles; Ultrasound; Ultrasound contrast agent.

ABSTRACT: The fabrication of an enzyme-degradable polymer/silica hybrid microbubble is reported that produces an ultrasound contrast image. The polymer, a triethoxysilane end-capped polycaprolactone (SiPCL), is used to incorporate enzyme-degradable components into a silica microbubble synthesis, and to impart increased elasticity for enhanced acoustic responsiveness. Formulations of 75, 85 and 95 wt% SiPCL in the polymer feed, produced quite similar ratios of SiPCL and silica in the final bubble but different surface properties. The data suggest that different regions of the microbubbles were SiPCL-rich: the inner layer next to the polystyrene template core and the outer surface layer, thereby creating a sandwiched silica-rich layer of the bubble shell. Overall, the thickness of the microbubble shell was dependent on the starting TEOS concentration and the reaction time. Despite the layered structure, the microbubble could be efficiently degraded by lipase enzyme, but was stable without enzyme. The ultrasound contrast showed a general trend of increase in image intensity with SiPCL feed ratio, although the 95 wt% SiPCL bubbles did not produce a contrast image, probably due to bubble collapse. At higher normalized peak negative acoustic pressure (mechanical index, MI), a non-linear frequency response also emerges, characterized by the third harmonic at around $3f_0$, and increases with MI. The threshold MI transition from linear to non-linear response increased with decrease in SiPCL.

1. Introduction

Ultrasound imaging is the second most common imaging modality used in clinics around the world, following x-ray imaging.[1,2] Ultrasound technology is safe, non-invasive, low risk, portable, offers results in real-time, and is relatively easy to use. Currently, ultrasound is used in applications involving the heart, vascular systems, abdominal organs, obstetrics, and is branching out into more advanced roles. These include molecular imaging, targeted drug delivery, opening the blood-brain barrier, and blood clot dissolution.[3–9]

Research on contrast agents has moved from "soft"-shelled agents, such as those made with lipids and proteins[10], into investigating the use of "rigid"-shelled microbubbles, to impart further stability to the gas bubble. The stronger shells of these rigid microbubbles means that their imaging life times are longer due to better stabilization of the shell, especially during oscillations. Additionally, the microbubbles can withstand higher pressures of ultrasound. However, the rigid shell also decreases the sensitivity of the microbubble to ultrasound insonation, at low ultrasound pressures. Moreover, it is very important for the rigid-shelled microbubbles to have a well-controlled size distribution, as unlike the soft-shelled microbubbles, they cannot deform to fit through small capillaries. Thus, the ideal size is 1-4μm, else, like whole particles, they could occlude the vessels.[11,12] Although nanobubbles might promote aggregation into tumor vasculature through the enhanced permeation and retention effect, the dependence of bubble echogenicity on its size, as well as the inability to fabricate relatively thin shells (thickness < 5% radius) that are capable of stabilizing the inner air bubble renders microbubbles the more attractive option for ultrasound contrast.[1,14]

Although emulsion techniques can result in a good yield, the control in size distribution of the microbubbles is improved by formation on a pre-characterized monodisperse sacrificial core template. For example, hollow silica microcapsules and microbubbles have been fabricated with this principle, by a sol-gel technique by Lu et al.[13] and Lin et al.[14] and, as reported by Walters and Hall[15], the use of a polystyrene microparticle sacrificial core, results in hollow silica microcapsules of great uniformity.

However, a pure silica shell made from tetraethyl orthosilicate (TEOS) was too brittle and cracked under high intensity insonation. By adding additional layers of long-chain organosilanes during the fabrication process, the shell was rendered more elastic and thus able to oscillate when ultrasound was applied.[14] Work has also been conducted with (3-aminopropyl)triethoxysilane to functionalize the microbubbles with amine groups for conjugation

with biomolecules for imaging, drug attachment, or targeting purposes.[16] Testing of these microbubbles *in vivo* and *in vitro* showed that the silica-based microbubbles can be imaged well.[14,16,17]

This opens the door to a dual function of contrast agent and drug delivery vehicle. Mesoporous silica with high surface area/volume ratio has been long established as an excellent material for drug delivery applications. Literature reports values of specific surface areas as high as 880 m^2/g and pore volumes over 1.5 cm^3/g. Thus, silica-based microbubbles might be expected to encapsulate high loads of therapeutics in the shell structure, despite having a hollow, air-filled, core.[18,19] Additionally, liquid filling, followed by evapouration leaves an inner 'skin' of additional material within the shell of the bubble. Mesoporous silica can also be easily functionalized, overall making it a good material to use for a multi-purpose vehicle.[20]

However, a drawback of using silica in short-term drug delivery is its slow biodegradation to silicic acid[21]. Thus, despite such promising properties for drug loading and as an ultrasound contrast agent, it is still lacking desirable *in vivo* properties.

As such, the work reported herein explores the potential for a biodegradable microbubble. Polycaprolactone (PCL) degradation occurs through the hydrolysis of ester linkages in its backbone.[22] Not only are the linkages susceptible to hydrolytic degradation, the rate can also be increased by enzymatic degradation, for example, from lipase enzymes.[23] As PCL is hydrophobic, the presence of lipase enzyme has been shown to speed up the degradation rate by over 1000 times.[23–25] On a macroscopic scale, implantation of PCL in rats showed that over 50% of the PCL had been excreted by the end of 60 days and only 9% remained after 120 days.[26] Without the presence of lipase, degradation of PCL is slow, with microparticles showing unchanged morphology even after 9 weeks, so that it is an attractive material in terms of potential shelf-life. Here, we report the development and characterization of an enzyme-degradable microbubble from silica and enzyme-degradable polymer SiPCL, with potential for future applications in simultaneous drug delivery and ultrasound contrast. Different formulations of microbubbles were fabricated and analyzed for their shell dimensions and compositions. Their ultrasound response is also reported in this paper.

2. Experimental

2.1 Materials

All chemicals were purchased from Sigma-Aldrich Company LLC (Dorset, UK), except for 6-hydroxyhaxanoic acid, which was purchased from Alfa Aesar (Johnson Matthey, Lancashire, UK). Lipase enzyme from *Pseudomonas cepacia* was also purchased from Sigma-Aldrich.

2.2 SiPCL Synthesis

The synthesis of SiPCL followed the protocol given by Tian et al.[27–29] The schematic of the reaction is shown in Figure 1. Polycaprolactone diol (PCL diol, M_n 2000 g/mol) was end-capped with alkoxysilane groups for sol-gel functionality using 3-(trimethoxysilyl)propyl isocyanate (IPTES) and 1,4-diazobicyclo[2,2,2]octane (DABCO). The molar ratio used was 1:3:2. PCL diol and DABCO were mixed and heated to 70°C in a round bottom flask under reflux. IPTES was added to start the reaction and the reaction was carried out for 22 – 24 hours. The product, SiPCL, was collected by precipitation in methanol and filtered before drying overnight by vacuum desiccation.

The synthesis of SiPCL was confirmed by the comparison of its FT-IR spectra to that published by Tian et al. and Rhee and colleagues, and to that of PCL diol.[27–32] Figure S.1 presents the FT-IR spectra of the 600 – 1600 cm^{-1} range with the chemical changes annotated. In this region, the Si-C stretch and Si-O-C bend were detected for the triethoxysilane end-cap, and the N-H and C-N bends of the urethane linkage were detected as well. In addition, the –NH stretch of the urethane linkage was detected at 3400 cm^{-1}, and the –OH stretch of the PCL diol disappeared.

Additionally, the measurement of molecular weight by gel permeation chromatography (GPC) confirmed the addition of the triethoxysilane end groups. The number average and weight average molecular weights were determined to be 8630 and 10035 g/mol while the PCL diol was determined to be 4484 and 6717 g/mol relative to the polystyrene standard. The large increase in molecular weight from PCL diol to SiPCL reflected the addition of large and bulky end-groups. Polymers with larger hydrodynamic volumes cannot enter the porous spaces in the gel of the GPC column and thus spend little time travelling through it.[33] Thus, the addition of end-cap was reflected as a significant increase in molecular weight.

Regarding the overestimation of PCL diol molecular weight as compared to the values reported by Sigma-Aldrich, it has been reported in literature that the molecular weight of aliphatic polymers such as PCL are overestimated when compared to a polystyrene calibration. A factor of 0.45 has been reported to correlate the molecular weight of polystyrene to PCL, and was successfully used here to compare PCL diol mass to that reported by the manufacturer.[34,35]

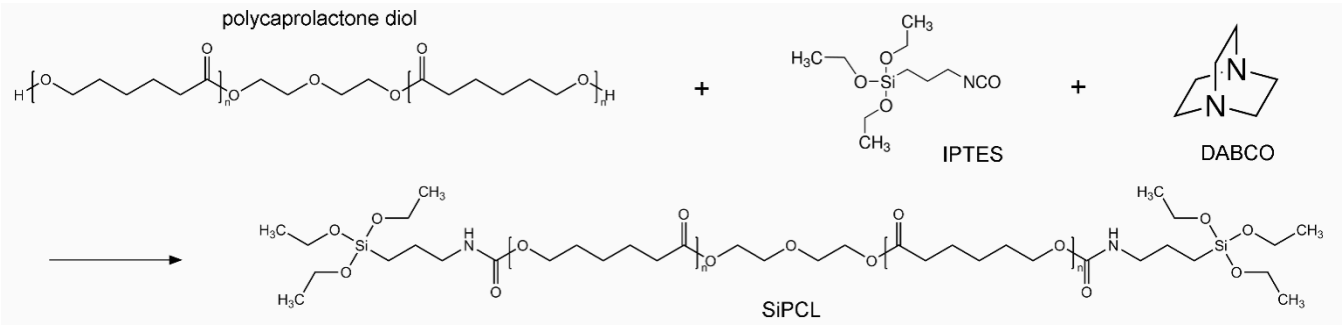

Figure 1: Schematic of the PCL diol end-capping reaction.

The addition of the end-caps was also confirmed with thermogravimetric analysis (TGA). The decomposition behavior of SiPCL was consistent with the addition of two triethoxysilane end-caps to PCL. Specifically, 90% of the initial mass was lost during the heating process, agreeing with the ratio of two remaining triethoxysilane groups and the loss of the 2000 g/mol PCL segment. Most of the mass loss occurred in the 200 – 500°C region, which was consistent with the thermal degradation of PCL as reported in literature.[36]

2.3 Polystyrene template synthesis

The polystyrene microparticle template was fabricated using dispersion polymerization according to Lin et al.[14] Ethanol (134 mL), water (6.9 mL), styrene (50.6 mL), 4-styrene sulfonic acid (0.37 g), poly(acrylic acid) (2.26 g), and azobisisobutyronitrile (1.0 g) were mixed together in a round bottom flask under reflux at low stirring speed and degassed by bubbling with N_2. The reaction was initiated by heating to 80°C and stopped at 24 hours by cooling with ice for 5 minutes. The polystyrene was collected by centrifugation and washed with ethanol. From TEM images, the polystyrene microparticles were observed to be spherical and uniform in size. Dynamic light scattering (DLS) measurements revealed near-monodisperse distribution, with a dispersity index of 0.226. The size of the microparticles was determined to be 2243 ± 65 nm by TEM imaging. To render the polystyrene positively charged, 0.5 w/v% polystyrene was incubated in 1 w/v% poly(allylamine hydrochloride) (PAH) solution. The excess PAH was washed off with water.

2.4 Sol-gel fabrication of SiPCL microbubbles

Microbubbles were synthesized using the modified Stöber sol-gel method as described by Lu et al. and Lin et al.[13,14] A typical reaction consisted of the following: isopropanol (20 mL), water (3.5 mL), ammonium hydroxide (0.5 mL), PAH-modified polystyrene (0.026 g), SiPCL (0.2 – 0.4 g) dissolved in 1 mL tetrahydrofuran (THF), and TEOS (0 – 214 µL). All chemicals except SiPCL and TEOS were first pre-mixed in an Erlenmeyer flask. To start the reaction, SiPCL solution was added dropwise, followed at 5 minutes by TEOS solution. The reaction was left to stir at room temperature for 5 hours, except for the 50 wt% SiPCL formulation, which was stopped at 3 hours. The reaction was terminated by removal from the solution through centrifugation. The resulting polystyrene/SiPCL/silica core/shell microparticles were washed with isopropanol, and the polystyrene was removed by incubation with THF. Vacuum desiccation was used to remove the THF and to fill the structure with air to form microbubbles.

2.5 Enzymatic degradation

SiPCL and SiPCL microbubble degradation was carried out at 37°C with shaking. The samples (10 mg) were suspended in 1 mL solution of 0.01 M phosphate buffered saline (PBS) with 200 – 300 U/L of lipase enzyme.

2.6 Chemical characterization methods

Fourier-transform infrared spectroscopy (FT-IR) was conducted on a Perkin Elmer Spectrum One FT-IR Spectrometer (Perkin Elmer Inc., MA, USA) with an attenuated total reflectance sampling accessory attached. The spectra was read from 550 – 4000 cm^{-1}.

GPC was conducted in chloroform on a Polymer Laboratories PL-GPC 50 Integrated GPC system (Varian Inc., MA, USA). A polystyrene standard was used.

Imaging of microbubbles was conducted using transmission electron microscopy (TEM) on a Technai G2 80-200 kV microscope (FEI, OR, USA) at 120 kV. Measurements were taken using ImageJ image processing software (National Institutes of Health, MD, USA).

Sessile drop contact angle measurements were made on approximately 8×10^7 microbubbles dried from 10 µL of microbubble solution to test the surface properties. A DataPhysics OCA 20 Contact Angle System (DataPhysics Instruments GmbH, Filderstadt, Germany) was used to monitor the change in 3 µL water droplets at a frame rate of 8.14 frames/second. The change in contact angle with respect to time was closely monitored over 30 seconds to determine the relative hydrophobicity between the samples. The change in contact angle within 1 second of droplet deposition was especially important in determining wettability, given the porous and loose nature of the microbubbles used for measurement.[37,38]

TGA was conducted on a LABSYS Evo (SETARAM Instrumentation UK, Caluire, France). Experiments were run from room temperature up to 700°C at a ramp rate of 5°C/minute.

DLS measurements were conducted on a Malvern Nano-ZS Zetasizer (Malvern Instruments Ltd., Worcestershire, UK).

Mass spectrometry was run in 50% aqueous acetonitrile under negative ion mode by the Mass Spectrometry Service at the Department of Chemistry, University of Cambridge (Cambridge, UK).

2.7 Ultrasound imaging

Imaging of the microbubbles was conducted using an Ultrasonix Sonix RP Ultrasound (Analogic Corporation, MA, USA). A linear 14 – 5 MHz, 38 mm transducer was used. Harmonic mode was used to image the microbubbles, at a center frequency of 5 MHz. Experiments were conducted with 400 mL of 1×10^9 microbubbles/L solution. The ultrasound response was collected using Stradwin ultrasound acquisition program (Department of Engineering, University of Cambridge, Cambridgeshire, UK). Both image intensity and radio frequency (RF) results were analyzed using MATLAB (MathWorks Inc., MA, USA).

3. Results and discussion

3.1 Microbubble design, synthesis and characterization

Attempts to produce microbubbles with PCL were not successful (data not shown), so that in itself it does not render a biodegradable bubble solution. However, introduction of the PCL via end-caps on SiPCL should offer both enzyme-degradability and easy incorporation into a silica matrix.[27] Good incorporation of SiPCL has been reported in bulk materials, and the degradation of SiPCL-containing materials has been shown to occur through the ester linkages of the polymer.[29,30,39] Degradation of PCL domains was the main cause of mass loss from the hybrid samples, and significantly increased the degradability of the samples over that of pure silica.[28,39] This is the same as the degradation of PCL.[36,40,41] In previous reports, the mass loss from degradation was found to be fast up to the end of 4 weeks, after which the degradation decreased slightly.[39]

SiPCL/silica hybrid microbubbles were fabricated here by sol-gel lamination of a sacrificial polystyrene core template. A product could be accomplished by adapting the classical sol-gel process for silica and silica/organosilica microbubbles as developed by Lu et al. and Lin et al.[13,14] Initial SiPCL concentrations of 50, 75, 85, and 95 wt% with respect to total SiPCL in SiPCL/TEOS were selected and microbubbles produced. These hybrid microbubbles were reproducibly uniform in size and shell thickness, as shown for example, in Figure 2.

As can be seen from Table 1, the shell thickness from any one formulation had a relatively small standard deviation, and different formulations were shown to be statistically different from each other ($p < 0.01$). A particularly thick shell was created when 50 wt% SiPCL (or greater TEOS content) was reacted for 5 hours. This revealed the expected differential reactivity of the TEOS with respect to the SiPCL, favoring TEOS incorporation over SiPCL, when it was present in excess. One option to increase SiPCL incorporation would be to maintain the PCL concentration in excess and gradually add TEOS over the period of fabrication (5 hours). However, the lamination approach from Lin et al.[13,14] offers versatility to create a microbubble with different layer properties. This may be suitable for creating SiPCL-rich layers as well as optimizing layers for future drug loading and delivery. Thus, in the data reported here, an initial charge of SiPCL was added to provide an inner layer and then the TEOS introduced after 5 mins. FT-IR spectra of the different microbubble formulations all contained an ester peak at 1728 cm^{-1}, confirming the addition of SiPCL to the microbubble shell. The spectra also contained silanol and silica peaks at 960 and 1045 cm^{-1} respectively, indicating the presence of a silica matrix (data not shown).

Table 1: SiPCL shell thickness measured from TEM images

Sample	Thickness (nm)	Time (hours)
50 wt% SiPCL	100 ± 13	5
50 wt% SiPCL	77 ± 4	3
75 wt% SiPCL	54 ± 2	5
85 wt% SiPCL	46 ± 1	5
95 wt% SiPCL	28 ± 2	5

From Table 1, there is a clear decease in shell thickness with increase in the initial weight percent of SiPCL in the lamination feed. This is consistent with a faster TEOS sol-gel process, than the incorporation of the end-capped SiPCL. To reduce the wall thickness for the 50 wt% SiPCL microbubbles, so that it was comparable with the other formulations, the reaction was stopped at 3 hours.

Figure 2 shows the thin shell around the spherical core and provides some insight into the different morphology with the different formulations. TEOS tends to polymerise into nano and micro-spherical structures of 50 nm to 2 μm in size, that grow to an aggregated microgel of polymer clusters, and thence coalesce.[42] In the case of polymerization onto a template surface, the sol particle clustering develops seeded from the surface. In the case of the microbubbles formed on a polystyrene template, the 50 – 85 wt% SiPCL microbubbles had the 'bumpy' surface suggesting a microcluster morphology that grows and merges together. This was highlighted at the defect sites in the shell – where the round edges suggested that shell growth was due to colloidal particles joining up together. On the other hand, the 95 wt% SiPCL microbubbles had less evidence of cluster mergence and the appearance of a more porous-like shell.

To investigate the incorporation of SiPCL into the microbubble shells, and check whether the lamination layers had been achieved, the reaction for 75 wt% SiPCL microbubbles was followed with time. It was found that the

contact angle changed during the reaction process (5 hours) although the bulk of the shell structure was created in the first hour. Combining the information from the shell thickness and contact angle results, inferred that the surface availability of SiPCL and silica changed throughout the reaction, resulting in layers of differing hydrophobicity. These results are illustrated by the scheme in Figure 3.

To interpret these results in terms of SiPCL incorporation, the initial charge of SiPCL coats the polystyrene template rendering a hydrophobic surface. Up to 30 minutes, the shell was thin and hydrophobic, which was attributed to a dominance of SiPCL, but the TEOS (added 5 minutes after the SiPCL) begins to dominate the surface of the structure by 1 hour (despite SiPCL still being available in solution), and the shell becomes hydrophilic. The doubling of shell thickness and increase in hydrophilicity during this time can be attributed to the rapid condensation of TEOS with a significantly slower SiPCL contribution. The faster hydrolysis and condensation times of TEOS have been attributed to its smaller specific volume and lower steric crowding around the silicon atom.[43–45] The increasing incorporation of silica continued to 3 hours (the contact angle continued to decrease while the shell growth plateaued off to approach the final shell thickness). Further lamination from 3 – 5 hours provided negligible change in shell thickness but a significant increase in contact angle, consistent with a slow coating of the outside surface with SiPCL that was still residual in solution.

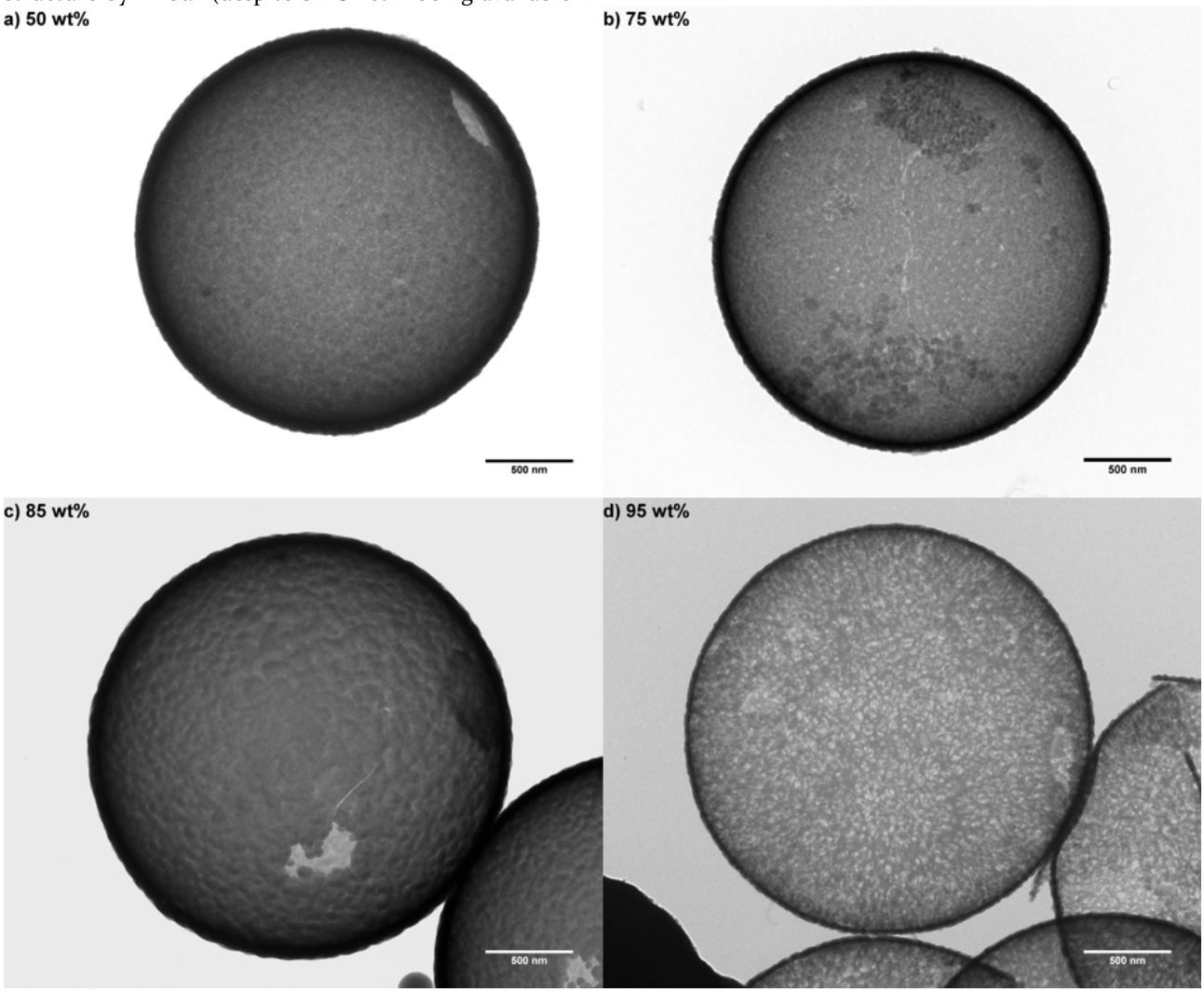

Figure 2: TEM images of a) 50, b) 75, c) 85, and d) 95 wt% SiPCL microbubbles.

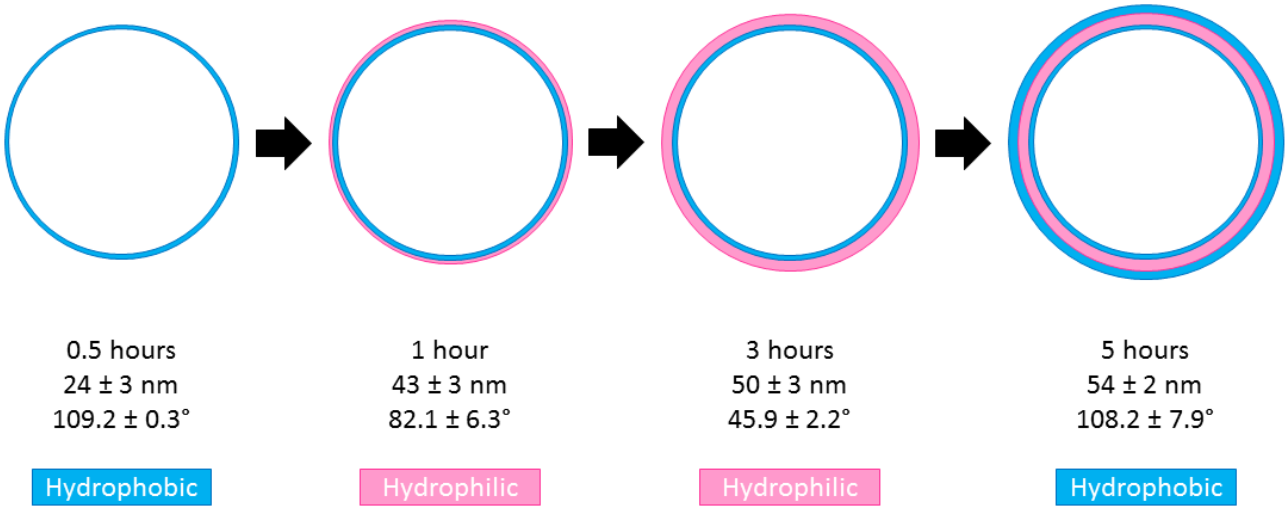

Figure 3: Schematic depicting the results obtained from stopping the 75 wt% SiPCL microbubble reaction at different times. The microbubbles were found to be hydrophobic at the beginning and at the end of the reaction with a middle hydrophilic layer that increased in thickness between 1 – 3 hours. (Layers in the schematic are not to scale.)

Leading from this layered lamination result, SiPCL coating on the outside of the capsule is predicted once the TEOS is depleted in the feed. The contact angles measured for the 75, 85 and 95 wt% SiPCL microbubbles were all over 100° and measurements were maintained over 30 seconds, providing further indication of a significant SiPCL presence on the surfaces of these microbubbles. In contrast, the 3 hour 50 wt% SiPCL microbubbles were hydrophilic, with contact angles measured, dropping from 104.7 ± 2.1° to 86.4 ± 4.1° after 1 second. The high initial contact angle for the 50 wt% SiPCL microbubbles demonstrated that the microbubbles still had hydrophobic properties due to exposed surface SiPCL in the early stages of lamination (also observed in the TEM image as patches of polymer on the surface), but the quick wetting and hydrophilic equilibrium contact angle in the final product showed that the surface also presented a hydrophilic interaction. For these microbubbles, the lowered contact angle and easy wetting indicated that the 3 hour 50 wt% SiPCL did not have a significant protective SiPCL-rich outer layer.

Since this interpretation assumes a differential rate of sol-gel incorporation, the final incorporation may not reflect the feed ratio. Thus, TGA was performed on the microbubbles to determine the final incorporation ratio. The incorporation was calculated from the mass loss of SiPCL and is presented in Table 2; it ranged from ~17wt% for the 50 wt% formulation, to ~26wt% for the 95 wt% SiPCL formulation and shows that SiPCL incorporation is nearly independent of feed ratio for formulations between 75 – 95 wt% SiPCL.

The microbubbles exhibited a similar but slightly broader mass loss temperature range compared with the pure polymer. In Figure 4a, the normalized derivatives of the mass-loss curves are presented. The mass loss onset temperature for the microbubbles was lower than the pure polymer; this has previously been attributed to size[46]: < 3 μm for the microbubbles compared with the macroscopic flakes of pure polymer. There is also a less well-defined second peak at higher temperature (up to 5 wt% of the total microbubble); this may reflect the initial SiPCL coating inside the microbubble and its different temperature profile, due to the combination of two possible mechanisms: decomposition products, hindered from leaving the sample by the silica-rich layer over the inner PCL layer, or the surrounding silica matrix may act as a thermal barrier in delaying polymer decomposition by stabilizing the polymer segments.[47,48]

Thus, the two peaks are consistent with SiPCL availability in the surface layer of the microbubbles and an inner SiPCL-rich layer (from the initial SiPCL charge in the microbubble formation). In the TGA trace, the second shoulder was observed between 400 – 500°C. This was less dominant than the main peak in the 75 – 95 wt% feed SiPCL, where the resultant microbubbles have a similar SiPCL incorporation. In contrast, in the 50 wt% SiPCL microbubbles, where the co-incorporation of SiPCL with TEOS is expected to be low the 'main' peak is reduced in size relative to the higher temperature peak (Figure 4b).

Table 2: Weight percent SiPCL incorporated into microbubble shell

Sample	Wt% Lost	SiPCL Wt%
SiPCL	90.7	100
50 wt% SiPCL	16.1	17.7
75 wt% SiPCL	21.2	23.3
85 wt% SiPCL	19.4	21.4
95 wt% SiPCL	23.9	26.3

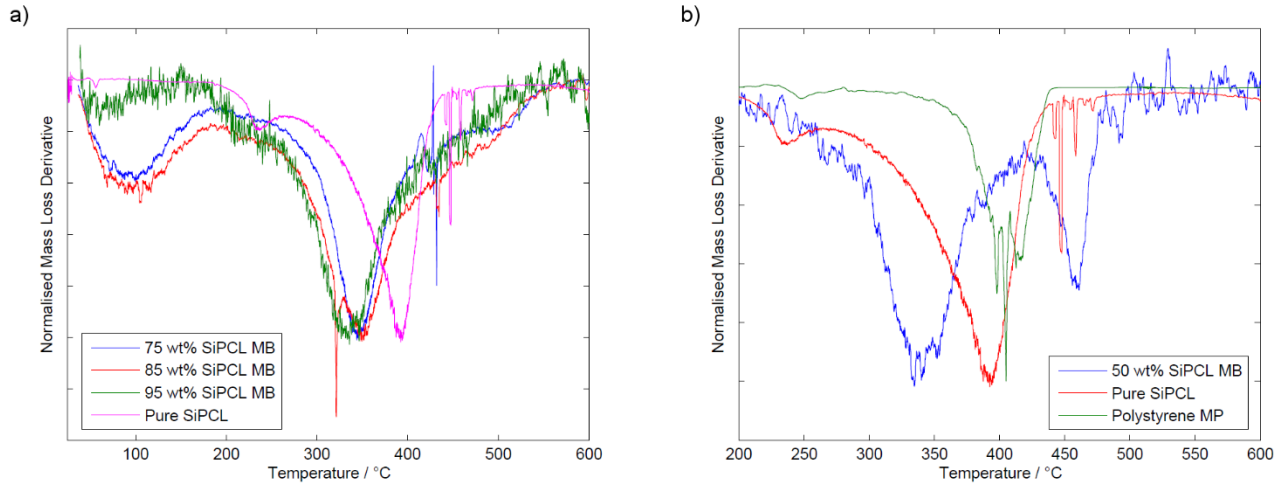

Figure 4: a) Derivatives of the mass loss curves of 75, 85, 95 wt% SiPCL microbubbles, and pure SiPCL polymer with respect to temperature. b) Derivatives of the mass loss curves for 50 wt% SiPCL microbubbles, SiPCL polymer, and polystyrene microparticles. All peaks are normalized for comparison of peak position.

The polystyrene microparticle thermal degradation curve is also shown in Figure 4b and it can be seen that there is overlap with the SiPCL curve, so that we cannot distinguish between residual polystyrene and PCL. However, no evidence of polystyrene core residue could be seen in the TEM for the 75 – 95 wt% microbubbles. In contrast, TEM imaging of 50 wt% SiPCL microbubbles revealed that some had a "microrattle" structure (Figure 5f). This is probably due to incomplete etching of the polystyrene core microparticle in these thicker-shelled microbubbles.

Further contrast can be seen in the lower temperature TGA range (Figure 4a) assigned to the evaporation of physically adsorbed water from the silica regions of the microbubble.[49,50] This is evident for 50 wt% (not shown) 75 and 85 wt% SiPCL and is consistent with the hygroscopic silica within the shell. In contrast, there was no mass loss from pure SiPCL and the 95 wt% SiPCL microbubbles. This difference suggested that the SiPCL and 95 wt% SiPCL microbubbles were predominantly hydrophobic.

3.2 Microbubble ultrasound response

Ultrasound images taken of the microbubbles under harmonic mode imaging were analyzed for pixel intensity and the frequency spectra of their response. Ultrasound intensity was characterized in terms of mechanical index (MI), a metric defined as the ratio of the peak negative pressure of the ultrasound (in MPa) to the square root of the center frequency (in MHz).

Ultrasound images (Figure 5b – e) were used to generate image intensity response curves and found to vary between formulations of 50 – 85 wt% SiPCL microbubbles. Interestingly the 95 wt% SiPCL microbubble showed very little response. The effect of shell properties on the ultrasound responsiveness of encapsulated microbubbles has been studied and modeled extensively. Specifically, shell elasticity and viscosity terms have been crucial in differentiating the modeling of shelled microbubbles under ultrasound insonation.[51–54] These terms affect the oscillatory behavior of the shell when insonated, which in turn reflects upon the backscatter generated.[55] For silica-based microbubbles, Lin et al.[14] showed that their acoustic activity was improved by a shell of increased elasticity. However, the TEM of the 95% SiPCL bubbles (Figure 5g) shows that, despite these microbubble shells being very thin (29 nm) and having increased elasticity, the bubbles collapse. In previous work[14] we found that "sticky" thin walled polymers with low T_g tended to collapse during drying, due to adhesion between opposite walls of the bubble. In cases where the adhesion predominated, re-inflation was prevented and so the bubble did not form to respond to insonation.

The other results presented in Figure 5 showed a general trend of increase in image intensity with SiPCL feed ratio which could suggest that shell elasticity increased with increasing initial SiPCL content, in line with the TGA predicted SiPCL content (17.7, 23.3 and 21.4 wt% respectively for 50, 75, 85 wt%) and estimated shell thickness (77, 54, 46 nm respectively), which has also been shown to play a role in determining the viscous damping of the acoustic signal in microbubbles, and thus the response collected.[56] It can also be seen that the 50 wt% SiPCL provided an image intensity which is very close to the silane microbubble (following the formulation reported by Walters and Hall[15]) which indicates that even small additions of SiPCL can increase image intensity.

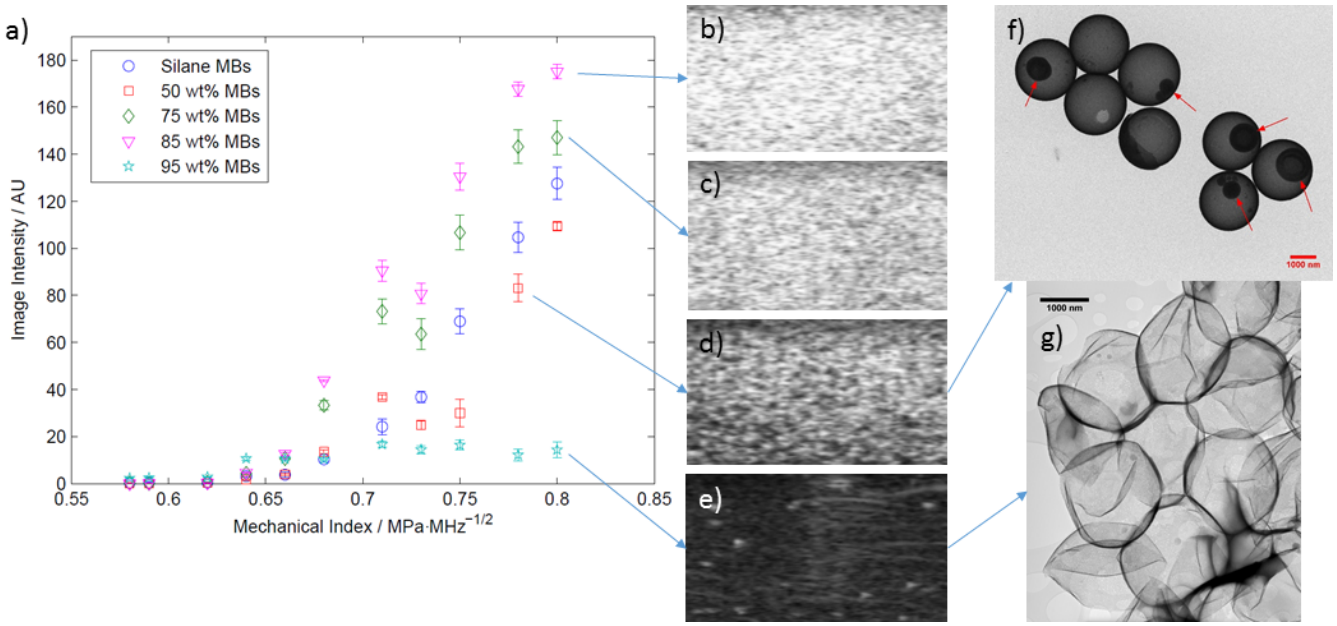

Figure 5: a) Image intensity response with respect to MI for silane and 50 – 95 wt% SiPCL microbubbles with representative ultrasound images for each formulation (b) 85 wt%, c) 75 wt%, d) 50 wt% and e) 95 wt% SiPCL) at the highest MI (MI 0.80). f) TEM micrograph showing "microrattle" structure of the 50 wt% SiPCL microbubbles, and g) TEM micrograph showing crumped 95 wt% SiPCL microbubbles.

Measurements of amorphous polymer thin film elasticity has shown that the elastic modulus varies as a function of film thickness, below a certain critical thickness. When the film is sufficiently thin (as in the case here) a surface layer of polymer with significantly lower Young's modulus will dominate the response.[57,58] Since the result is a higher intensity ultrasound image, this is encouraging for the formulation proposed, particularly in view of its potential for natural biodegradation through lipase action in the blood stream.

The RF signal in this MI range also provides information on the harmonics and can reveal the conditions where transition occurs from a linear to non-linear response. Figure 6 shows the response of 85 wt% SiPCL microbubbles at MI 0.71 and shows that at low MI a peak centered ~6MHz could be deconvolved into a peak around the 5Mhz fundamental response (f_o) and a shoulder at $3/2f_o$. This has been seen previously in other contrast agents, and believed to derive from the beat phenomenon caused by the combination of f_o and $2f_o$.[59–61] At higher MI, the non-linear response also emerges, characterized by the third harmonic at around $3f_o$, and increases with MI. The threshold MI (between 0.75-0.80) for this harmonic is dependent on formulation (Figure 7), so, for example, at MI 0.71 none of the formulations show non-linear behavior; at MI 0.75 only the 85% SiPCL produces a non-linear response and at 0.78 only the 50% SiPCL formulation is *without* a non-linear signal (95% is very weak as discussed above).

Overall, the ability of the SiPCL microbubbles to be imaged extensively under harmonic mode at high MIs was promising for highly stable and biodegradable microbubbles for use with high intensity ultrasound. Commercial agents already start responding at MIs as low as MI 0.07 and barely survive more than two ultrasound pulses.[14,62] The SiPCL microbubble imaging results were obtained over multiple pulses of ultrasound. Over 5 seconds of ultrasound was applied at each MI and the recordings were taken consecutively on the same sample without replenishment. The increased stability and lack of inertial cavitation at high MIs may limit the drug delivery capabilities through microbubble rupture, but could be highly efficient as a drug carrier vehicle for sustained drug delivery.

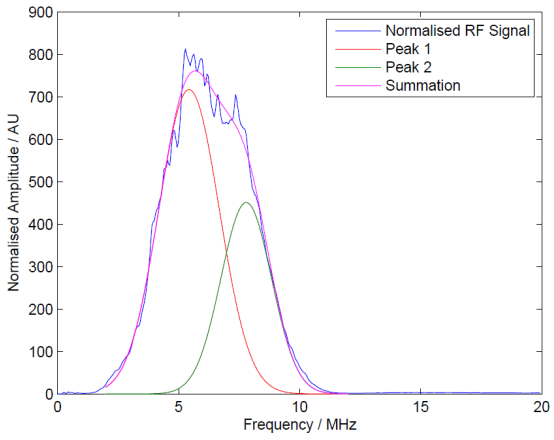

Figure 6: Frequency spectra of 85 wt% SiPCL microbubbles at MI 0.71, with deconvoluted f_o and $3/2f_o$ responses highlighted as "Peak 1" and "Peak 2" respectively.

3.3 SiPCL hydrolytic degradation

Degradation of PCL results in the release of hydrolysis products 6-hydroxyhexanoic acid, caprolactone, and cyclic

dimers and trimers of caprolactone.[63,64] These products, together with a change in solution pH can provide information about the degradation process.

Figure 8 compares the pH profile for SiPCL degradation with and without the presence of the enzyme, lipase. It shows that after an initial increase in pH after placing SiPCL in buffer solution, the pH measured returned to the starting buffer pH of 7.45 over a period of 5 days. In contrast, enzyme catalyzed degradation of SiPCL, investigated by incubation with lipase enzyme from *Pseudomonas cepacia* did not show any initial increase in pH and the decrease in pH (approximately 0.2 pH units over 5 days) was equivalent to approx. 13 µmol of monomer released from approx. 80 µmol polymer (0.2 g). Investigation of the release products by mass spectrometry revealed that while the monomer was detected in the enzyme catalyzed sample (at 131.07 m/z), no peaks were observed for the SiPCL in buffer solution.

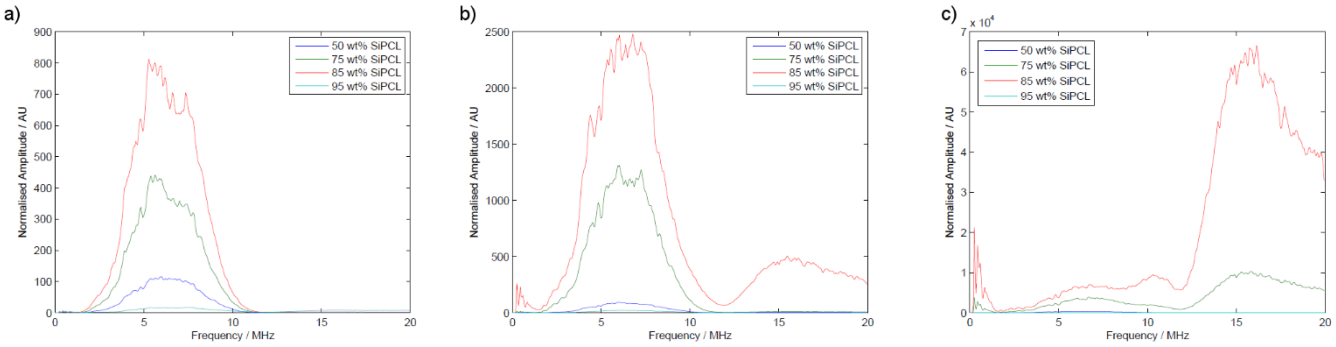

Figure 7: RF spectra of 50 – 95 wt% SiPCL microbubbles at a) MI 0.71, b) MI 0.75, and c) MI 0.78.

It has been shown previously that after 72 hours of incubation with lipase solution, up to 80 wt% of PCL film may be degraded.[23] It has also been reported that hydrolysis of PCL occurs in a linear-monomeric action from chain ends, but the PCL segment in SiPCL here is end-capped by triethoxysilane.[26] As such, mid-chain cleavage has to occur to expose PCL segments for degradation. This may protect the polymer from background hydrolysis, giving it shelf-life but still achieving lipase catalyzed degradation.

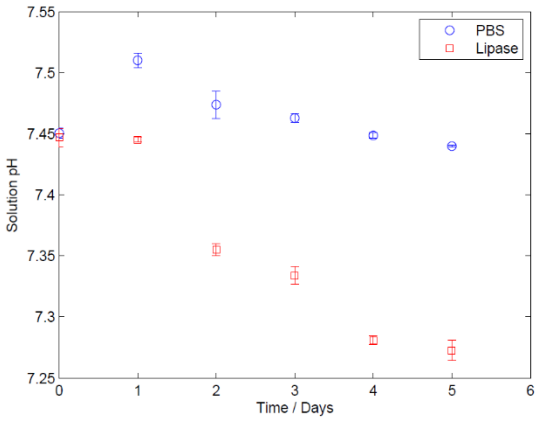

Figure 8: Supernatant pH of SiPCL samples exposed to hydrolytic (PBS) and both hydrolytic and enzymatic (lipase) degradation.

Investigation of microbubble degradation showed similar results to those obtained from degradation of pure SiPCL. Due to the low wt% of SiPCL in microbubbles and the large amount of microbubbles required for a noticeable change to be detected by pH, degradation studies were only conducted by mass spectrometry. Degradation of 50 wt% SiPCL microbubbles by hydrolytic scission failed to generate detectable 6-hydroxyhexanoic monomer by the end of 5 days of incubation. However, even for this low SiPCL loading, the addition of lipase significantly sped up the degradation process. By Day 4 of enzymatic degradation, a 6-hydroxyhexanoic acid monomer peak was detected by mass spectrometry. This peak further increased in intensity between Day 4 and Day 5.

These findings were reinforced by the TEM images. Figure 9 compares enzymatic, and hydrolytic degradation and shows the shells appeared highly porous after enzyme catalyzed hydrolysis. In contrast, microcapsules that had only been exposed to hydrolytic degradation remained morphologically similar to untreated microcapsules. In cross section (Figure 9) these differences are emphasized. From measurements taken of the shell thickness before and after hydrolysis, it was found that a reduction was found during enzyme treatment, from 77 ± 4 nm to 65 ± 4 nm. This compares with a thickness after hydrolytic cleavage of 71 ± 5 nm. Atomic force microscope images of bulk SiPCL/silica surfaces have been shown to contain large pores after 8 days of enzymatic degradation.[29]

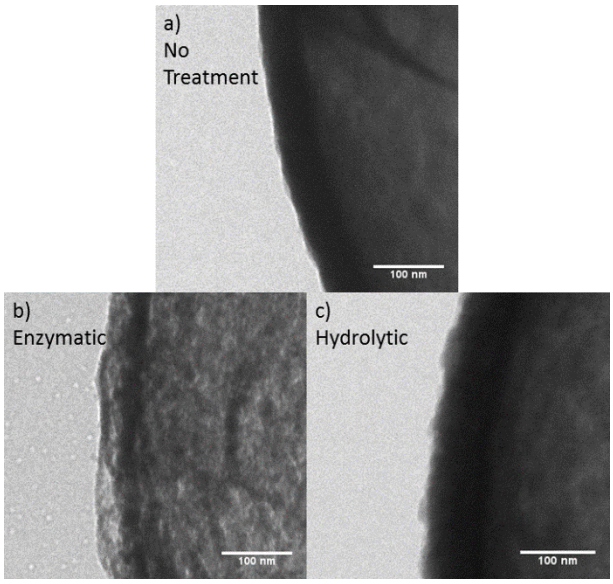

Figure 9: TEM images of 50 wt% SiPCL microcapsules with a) no treatment, b) enzymatic degradation, and c) hydrolytic degradation.

4. Conclusions

This work shows that an enzyme-degradable polymer with triethoxysilane end-caps can be repurposed for fabrication of enzyme-degradable ultrasound contrast microbubbles, when incorporated in a silica sol-gel process. The polymer/silica hybrid microbubbles could be fabricated to high uniformity in size and shell thickness and by introducing the SiPCL in advance of the TEOS to allow pre-coating of the the polystyrene core template, the microbubbles were shown to contain SiPCL in SiPCL-rich layers in the structure, although most of the material was characterized as silica-rich. Despite the gradiaent in SiPCL through the shell, enzymatic degradation with lipase was effective, rendering a rather 'open' porous structure. These microbubbles were shown to be acoustically responsive to ultrasound. The acoustic response of the microbubbles was found to be correlated with the SiPCL/TEOS ratio in the sol-gel feed and thus the shell thickness, elasticity and damping ability of the shell. Overall, the SiPCL/silica microbubbles were found to be highly stable under ultrasound insonation and offer an interlinked gradient of hydrophobic and hydrophilic areas that that could be used for selective drug loading, as will be reported shortly.

ASSOCIATED CONTENT

Supporting Information. FT-IR spectra of PCL diol and synthesized SiPCL. This material is available free of charge via the Internet at http://pubs.acs.org.

AUTHOR INFORMATION

Corresponding Author

Elizabeth A H Hall

Institute of Biotechnology, Department of Chemical Engineering and Biotechnology, University of Cambridge
Tennis Court Road
Cambridge, CB2 1QT
lisa.hall@biotech.cam.ac.uk

Author Contributions

The manuscript was written through contributions of all authors. All authors have given approval to the final version of the manuscript.

ABBREVIATIONS

DABCO, 1,4-diazobicyclo[2,2,2]octane; DLS, dynamic light scattering; f_0, fundamental frequency; FT-IR, Fourier-transform infrared spectroscopy; GPC, gel permeation chromatography; IPTES, 3-(trimethoxysilyl)propyl isocyante; MI, mechanical index; PAH, poly(allylamine hydrochloride); PBS, phosphate buffered saline; PCL, polycaprolactone; RF, radio frequency; SiPCL, triethoxysilane end-capped polycaprolactone; TEM, transmission electron microscopy; TEOS, tetraethyl orthosilicate; TGA, thermogravimetric analysis; THF, tetrahydrofuran.

REFERENCES

(1) Schutt, E. G.; Klein, D. H.; Mattrey, R. M.; Riess, J. G. Injectable Microbubbles as Contrast Agents for Diagnostic Ultrasound Imaging: The Key Role of Perfluorochemicals. *Angew. Chem. Int. Ed. Engl.* **2003**, *42* (28), 3218–3235.

(2) Hahn, M. A.; Singh, A. K.; Sharma, P.; Brown, S. C.; Moudgil, B. M. Nanoparticles as Contrast Agents for in-Vivo Bioimaging: Current Status and Future Perspectives. *Anal. Bioanal. Chem.* **2011**, *399* (1), 3–27.

(3) Lentacker, I.; De Smedt, S. C.; Sanders, N. N. Drug Loaded Microbubble Design for Ultrasound Triggered Delivery. *Soft Matter* **2009**, *5* (11), 2161–2170.

(4) Coussios, C. C.; Roy, R. A. Applications of Acoustics and Cavitation to Noninvasive Therapy and Drug Delivery. *Annu. Rev. Fluid Mech.* **2008**, *40* (1), 395–420.

(5) Rapoport, N. Ultrasound-Mediated Micellar Drug Delivery. *Int. J. Hyperthermia* **2012**, *28* (4), 374–385.

(6) Sirsi, S. R.; Borden, M. A. Advances in Ultrasound Mediated Gene Therapy Using Microbubble Contrast Agents. *Theranostics* **2012**, *2* (12), 1208–1222.

(7) Hitchcock, K. E. Ultrasound-Assisted Thrombolysis for Stroke Therapy: Better Thrombus Break-up with Bubbles. *Stroke* **2010**, *41* (10 Suppl), S50–S53.

(8) Stride, E. P.; Coussios, C. C.; Wells, P. N. T. Cavitation and Contrast: The Use of Bubbles in Ultrasound Imaging and Therapy. *Proc. Inst. Mech. Eng. Part H J. Eng. Med.* **2010**, *224* (2), 171–191.

(9) Choi, J. J.; Feshitan, J. A.; Baseri, B.; Wang, S.; Tung, Y.-S.; Borden, M. A.; Konofagou, E. E. Microbubble-Size Dependence of Focused Ultrasound-Induced Blood-Brain Barrier Opening in Mice in Vivo. *IEEE Trans. Biomed. Eng.* **2010**, *57* (1), 145–154.

(10) Stride, E.; Tang, M.-X.; Eckersley, R. J. Physical Phenomena Affecting Quantitative Imaging of Ultrasound Contrast Agents. *Appl. Acoust.* **2009**, *70* (10), 1352–1362.

(11) Straub, J. A.; Chickering, D. E.; Church, C. C.; Shah, B.; Hanlon, T.; Bernstein, H. Porous PLGA Microparticles: AI-700, an Intravenously Administered Ultrasound Contrast Agent for Use in Echocardiography. *J. Control. Release* **2005**, *108* (1), 21–32.

(12) Lensen, D.; Gelderblom, E. C.; Vriezema, D. M.; Marmottant, P.; Verdonschot, N.; Versluis, M.; de Jong, N.; van Hest, J. C. M. Biodegradable Polymeric Microcapsules

for Selective Ultrasound-Triggered Drug Release. *Soft Matter* **2011**, *7* (11), 5417–5422.
(13) Lu, Y.; McLellan, J.; Xia, Y. Synthesis and Crystallization of Hybrid Spherical Colloids Composed of Polystyrene Cores and Silica Shells. *Langmuir* **2004**, *20* (8), 3464–3470.
(14) Lin, P.-L.; Eckersley, R. J.; Hall, E. A. H. Ultrabubble: A Laminated Ultrasound Contrast Agent with Narrow Size Range. *Adv. Mater.* **2009**, *21* (38-39), 3949–3952.
(15) Walters, J. D.; Hall, E. A. H. An Optrode Particle Geometry to Decrease Response Time. *Analyst* **2011**, *136*, 4718–4723.
(16) Hu, H.; Zhou, H.; Du, J.; Wang, Z.; An, L.; Yang, H.; Li, F.; Wu, H.; Yang, S. Biocompatible Hollow Silica Microspheres as Novel Ultrasound Contrast Agents for in Vivo Imaging. *J. Mater. Chem.* **2011**, *21* (18), 6576–6583.
(17) Martinez, H. P.; Kono, Y.; Blair, S. L.; Sandoval, S.; Wang-Rodriguez, J.; Mattrey, R. F.; Kummel, A. C.; Trogler, W. C. Hard Shell Gas-Filled Contrast Enhancement Particles for Colour Doppler Ultrasound Imaging of Tumors. *Medchemcomm* **2010**, *1* (4), 266–270.
(18) Margolese, D.; Melero, J. a.; Christiansen, S. C.; Chmelka, B. F.; Stucky, G. D. Direct Syntheses of Ordered SBA-15 Mesoporous Silica Containing Sulfonic Acid Groups. *Chem. Mater.* **2000**, *12* (8), 2448–2459.
(19) Guo, H.; Qian, H.; Sun, S.; Sun, D.; Yin, H.; Cai, X.; Liu, Z.; Wu, J.; Jiang, T.; Liu, X. Hollow Mesoporous Silica Nanoparticles for Intracellular Delivery of Fluorescent Dye. *Chem. Cent. J.* **2011**, *5* (1), 1.
(20) Slowing, I. I.; Trewyn, B. G.; Giri, S.; Lin, V. S.-Y. Mesoporous Silica Nanoparticles for Drug Delivery and Biosensing Applications. *Adv. Funct. Mater.* **2007**, *17* (8), 1225–1236.
(21) Finnie, K. S.; Waller, D. J.; Perret, F. L.; Krause-Heuer, A. M.; Lin, H. Q.; Hanna, J. V.; Barbé, C. J. Biodegradability of Sol-Gel Silica Microparticles for Drug Delivery. *J. Sol-Gel Sci. Technol.* **2008**, *49* (1), 12–18.
(22) Göpferich, A. Mechanisms of Polymer Degradation and Erosion. *Biomaterials* **1996**, *17* (2), 103–114.
(23) Li, S.; Liu, L.; Garreau, H.; Vert, M. Lipase-Catalyzed Biodegradation of Poly(ε-Caprolactone) Blended with Various Polylactide-Based Polymers. *Biomacromolecules* **2003**, *4* (2), 372–377.
(24) Chawla, J. S.; Amiji, M. M. Biodegradable Poly(ε-Caprolactone) Nanoparticles for Tumor-Targeted Delivery of Tamoxifen. *Int. J. Pharm.* **2002**, *249* (1-2), 127–138.
(25) Chen, D. R.; Bei, J. Z.; Wang, S. G. Polycaprolactone Microparticles and Their Biodegradation. *Polym. Degrad. Stab.* **2000**, *67* (3), 455–459.
(26) Pitt, C. G.; Chasalow, F. I.; Hibionada, Y. M.; Klimas, D. M.; Schindler, A. Aliphatic Polyesters. I. The Degradation of Poly(ε-Caprolactone) In Vivo. *J. Appl. Polym. Sci.* **1981**, *26*, 3779–3787.
(27) Tian, D.; Dubois, P.; Jerome, R. A New Poly(ε-Caprolactone) Containing Hybrid Ceramer Prepared by the Sol-Gel Process. *Polymer (Guildf).* **1996**, *37* (17), 3983–3987.
(28) Rhee, S.-H.; Choi, J.-Y.; Kim, H.-M. Preparation of a Bioactive and Degradable Poly(ε-Caprolactone)/silica Hybrid through a Sol-Gel Method. *Biomaterials* **2002**, *23* (24), 4915–4921.
(29) Tian, D.; Dubois, P.; Grandfils, C.; Jerome, R.; Viville, P.; Lazzaroni, R.; Bredas, J.-L.; Leprince, P. A Novel Biodegradable and Biocompatible Ceramer Prepared by the Sol-Gel Process. *Chem. Mater.* **1997**, *9* (4), 871–874.
(30) Rhee, S.-H.; Lee, Y.-K.; Lim, B.-S.; Yoo, J. J.; Kim, H. J. Evaluation of a Novel Poly(ε-Caprolactone)-Organosiloxane Hybrid Material for the Potential Application as a Bioactive and Degradable Bone Substitute. *Biomacromolecules* **2004**, *5* (4), 1575–1579.
(31) Song, S.-H.; Lee, S. J.; Rhee, S.-H. Synthesis of Biodegradable Poly(ε-Caprolactone)-Organosiloxane Hybrid with Carboxylate Groups. *J. Biomed. Mater. Res. Part B Appl. Biomater.* **2012**, *100* (5), 1289–1297.
(32) Yoo, J. J.; Rhee, S.-H.; Lee, J. Il; Kim, H. J. Evaluations of Bioactive Poly(ε-Caprolactone)-Organosiloxane Nano-Hybrid as a Material for Bone Repair. *Tissue Eng. Regen. Med.* **2009**, *6* (4-11), 445–452.
(33) Su, W.-F. Polymer Size and Polymer Solution. In *Principles of Polymer Design and Synthesis*; Springer, 2013; pp 9–26.
(34) Baez, J. E.; Martinez-Richa, A.; Marcos-Fernandez, A. One-Step Route to α-Hydroxyl-ω-(Carboxylic Acid) Polylactones Using Catalysis by Decamolybdate Anion. *Macromolecules* **2005**, *38* (5), 1599–1608.
(35) Huang, C.-H.; Wang, F.-C.; Ko, B.-T.; Yu, T.-L.; Lin, C.-C. Ring-Opening Polymerization of ε-Caprolactone and L-Lactide Using Aluminum Thiolates as Initiator. *Macromolecules* **2001**, *34*, 356–361.
(36) Elzubair, A.; Elias, C. N.; Suarez, J. C. M.; Lopes, H. P.; Vieira, M. V. B. The Physical Characterization of a Thermoplastic Polymer for Endodontic Obturation. *J. Dent.* **2006**, *34* (10), 784–789.
(37) Andre, V.; Zosel, A. Dynamic Wetting on Porous and Non Porous Substrates. Influence of Surface Tension, Viscosity and Porosity. *Berichte der Bunsengesellschaft für Phys. Chemie* **1994**, *98* (3), 429–434.
(38) Buckton, G.; Newton, J. M. Liquid Penetration as a Method of Assessing the Wettability and Surface Energy of Pharmaceutical Powders. *J. Pharm. Pharmacol.* **1986**, *38* (5), 329–334.
(39) Rhee, S.-H. Effect of Molecular Weight of Poly(ε-Caprolactone) on Interpenetrating Network Structure, Apatite-Forming Ability, and Degradability of Poly(ε-Caprolactone)/silica Nano-Hybrid Materials. *Biomaterials* **2003**, *24* (10), 1721–1727.
(40) Pitt, C. G.; Gu, Z. Modification of the Rates of Chain Cleavage of Poly(ε-Caprolactone) and Related Polyesters in the Solid State. *J. Control. Release* **1987**, *4*, 283–292.
(41) Bei, J.-Z.; Li, J.-M.; Wang, Z.-F.; Le, J.-C.; Wang, S.-G. Polycaprolactone - Poly(ethylene-Glycol) Block Copolymer. IV: Biodegradation Behavior in Vitro and in Vivo. *Polym. Adv. Technol.* **1997**, *8*, 693–696.
(42) Milea, C. A.; Bogatu, C. The Influence of Parameters in Silica Sol-Gel Process. *Bull. Transilv. Univ. Brasov Eng. Sci.* **2011**, *4* (1), 59–66.
(43) Chen, K. C.; Tsuchiya, T.; Mackenzie, J. D. Sol-Gel Processing of Silica I. The Role of the Starting Compounds. *J. Non. Cryst. Solids* **1986**, *81*, 227–237.
(44) Radi, B. Reinforced Hydrogels for Silicone Copolymer Delivery for Scar Remediation, Queensland University of Technology, 2010.
(45) Pouxvile, J. C.; Boilot, J. P. Kinetic Simulations and Mechanisms of the Sol-Gel Polyermization. *J. Non. Cryst. Solids* **1987**, *94*, 374–386.
(46) Martinez, E. The Effect of Particle Size on the Thermal Properties of Serpentine Minerals. *Am. Mineral.* **1961**, *46*, 901–912.
(47) Tien, Y. I.; Wei, K. H. The Effect of Nano-Sized Silicate Layers from Montmorillonite on Glass Transition, Dynamic Mechanical, and Thermal Degradation Properties of Segmented Polyurethane. *J. Appl. Polym. Sci.* **2002**, *86* (7), 1741–1748.
(48) Peng, Z.; Kong, L. X. A Thermal Degradation Mechanism of Polyvinyl Alcohol/silica Nanocomposites. *Polym. Degrad. Stab.* **2007**, *92* (6), 1061–1071.
(49) Wallace, S.; Hench, L. L. Structural Analysis of Water Adsorbed in Silica Gel. *J. Sol-Gel Sci. Technol.* **1994**, *1*, 153–168.
(50) Scott, R.; Traiman, S. Solute-Solvent Interactions on the Surface of Silica Gel:: III. Multilayer Adsorption of Water on the Surface of Silica Gel. *J. Chromatogr. A* **1980**, *196*, 193–205.
(51) de Jong, N.; Emmer, M.; Wamel, A.; Versluis, M. Ultrasonic Characterization of Ultrasound Contrast Agents. *Med. Biol.*

Eng. Comput. **2009**, *47* (8), 861–873.
(52) Postema, M.; Schmitz, G. Ultrasonic Bubbles in Medicine: Influence of the Shell. *Ultrason. Sonochem.* **2007**, *14* (4), 438–444.
(53) Frinking, P. J. A.; de Jong, N. Acoustic Modeling of Shell-Encapsulated Gas Bubbles. *Ultrasound Med. Biol.* **1998**, *24* (4), 523–533.
(54) Hoff, L.; Sontum, P.; Hovem, J. Oscillations of Polymeric Microbubbles: Effect of the Encapsulating Shell. *J. Acoust. Soc. Am.* **2000**, *107* (4), 2272–2280.
(55) Sirsi, S.; Borden, M. Microbubble Compositions, Properties and Biomedical Applications. *Bubble Sci. Eng. Technol.* **2009**, *1* (1-2), 3–17.
(56) Mukdadi, O. M.; Kim, H.-B.; Hertzberg, J.; Shandas, R. Numerical Modeling of Microbubble Backscatter to Optimize Ultrasound Particle Image Velocimetry Imaging: Initial Studies. *Ultrasonics* **2004**, *42* (10), 1111–1121.
(57) Ao, Z.; Li, S. Temperature- and Thickness-Dependent Elastic Moduli of Polymer Thin Films. *Nanoscale Res. Lett.* **2011**, *6* (1), 243.
(58) Stafford, C. M.; Vogt, B. D.; Harrison, C.; Julthongpiput, D.; Huang, R. Elastic Moduli of Ultrathin Amorphous Polymer Films. *Macromolecules* **2006**, *39* (15), 5095–5099.
(59) de Jong, N.; Bouakaz, A.; Frinking, P. Harmonic Imaging with Ultrasound Contrast Agents. *2000 IEEE Ultrason. Symp.* **2000**, 1869–1876.
(60) Husseini, G. A.; Diaz de la Rosa, M. A.; Richardson, E. S.; Christensen, D. A.; Pitt, W. G. The Role of Cavitation in Acoustically Activated Drug Delivery. *J. Control. Release* **2005**, *107* (2), 253–261.
(61) Basude, R.; Wheatley, M. a. Generation of Ultraharmonics in Surfactant Based Ultrasound Contrast Agents: Use and Advantages. *Ultrasonics* **2001**, *39* (6), 437–444.
(62) Thomas, D. H.; Looney, P.; Butler, M.; Anderson, T.; McDicken, W. N.; Sboros, V.; Pelekasis, N. The Fate of Resonant and off-Resonant Microbubble Signals in Response to Consecutive Imaging Pulses. *2010 IEEE Int. Ultrason. Symp.* **2010**, 1712–1715.
(63) Hakkarainen, M.; Albertsson, A.-C. Heterogeneous Biodegradation of Polycaprolactone - Low Molecular Weight Products and Surface Changes. *Macromol. Chem. Phys.* **2002**, *203* (10-11), 1357–1363.
(64) Abe, H.; Doi, Y.; Aoki, H.; Akehata, T.; Hori, Y.; Yamaguchi, A. Physical Properties and Enzymatic Degradability of Copolymers of (R)-3-Hydroxybutyric and 6-Hydroxyhexanoic Acids. *Macromolecules* **1995**, *28*, 7630–7637.

SYNOPSIS TOC (Word Style "SN_Synopsis_TOC"). If you are submitting your paper to a journal that requires a synopsis graphic and/or synopsis paragraph, see the Instructions for Authors on the journal's homepage for a description of what needs to be provided and for the size requirements of the artwork.

Authors are required to submit a graphic entry for the Table of Contents (TOC) that, in conjunction with the manuscript title, should give the reader a representative idea of one of the following: A key structure, reaction, equation, concept, or theorem, etc., that is discussed in the manuscript. Consult the journal's Instructions for Authors for TOC graphic specifications.

Insert Table of Contents artwork here

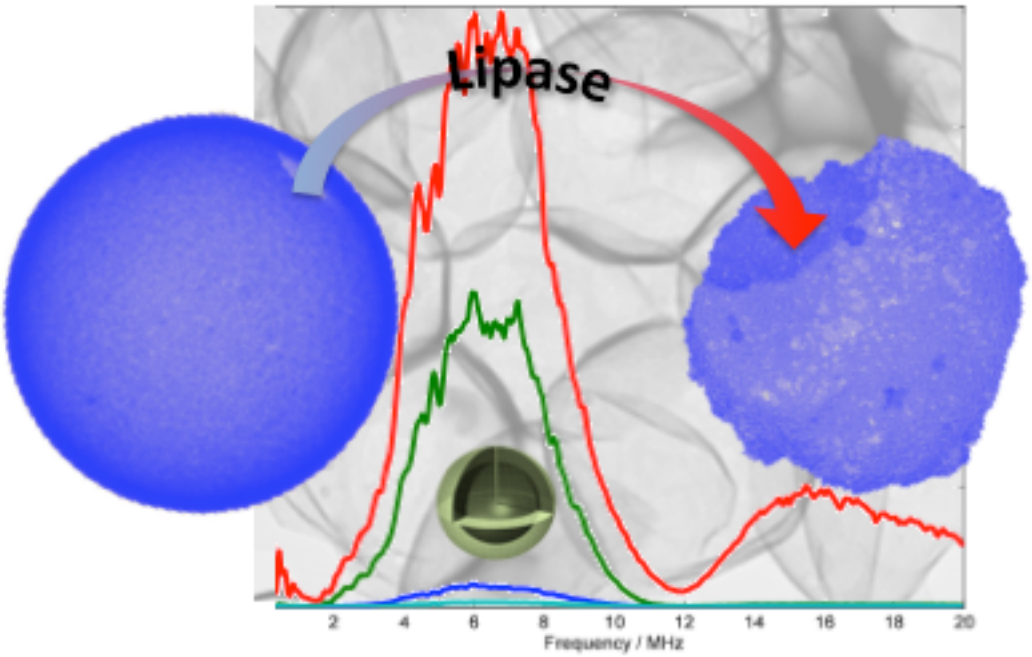

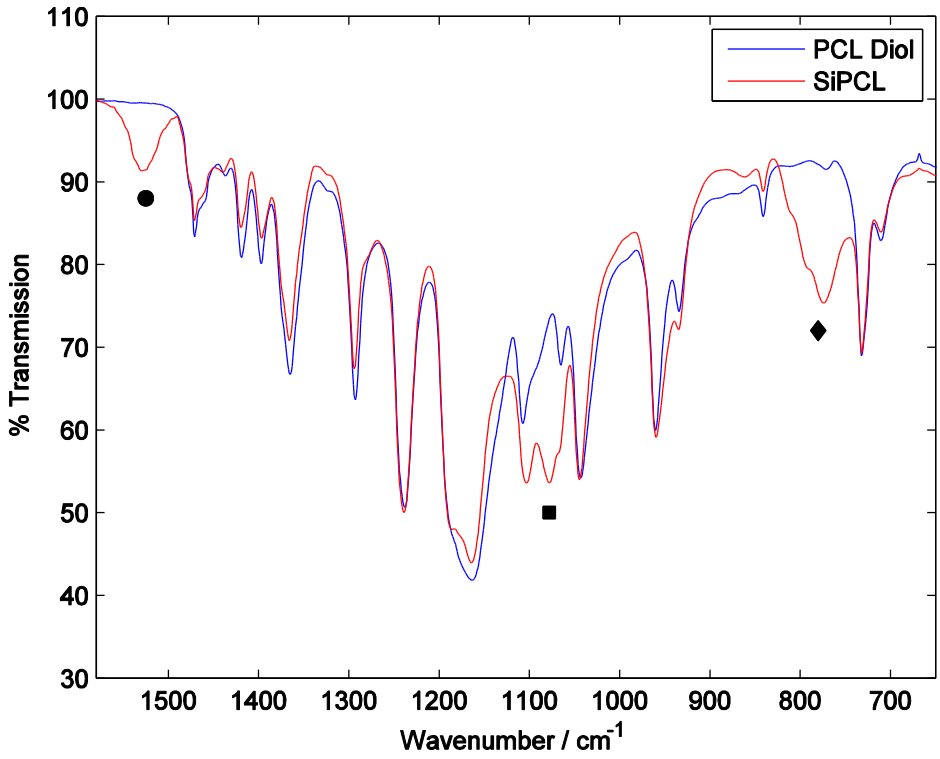

Figure S.1: FT-IR spectra of PCL diol (as supplied) and SiPCL synthesized. The SiPCL FT-IR spectra showed the appearance of an urethane linkage as determined by the N-H and C-N bend at 1525 cm^{-1} (●), and the appearance of the triethoxysilane end-cap by Si-O-C bend at 1078 cm^{-1} (■), and Si-C stretch at 780 cm^{-1} (♦).